Global Change Biology

Global Change Biology (2013) **19**, 2104–2116, doi: 10.1111/gcb.12172

Traceable components of terrestrial carbon storage capacity in biogeochemical models

JIANYANG XIA*, YIQI LUO*, YING-PING WANG† and OLEKSANDRA HARARUK*

Department of Microbiology and Plant Biology, University of Oklahoma, OK, USA, †CSIRO Marine and Atmospheric Research, Centre for Australian Weather and Climate Research, Aspendale, Victoria, Australia

Abstract

Biogeochemical models have been developed to account for more and more processes, making their complex structures difficult to be understood and evaluated. Here, we introduce a framework to decompose a complex land model into traceable components based on mutually independent properties of modeled biogeochemical processes. The framework traces modeled ecosystem carbon storage capacity (X_{ss}) to (i) a product of net primary productivity (NPP) and ecosystem residence time (τ_E). The latter τ_E can be further traced to (ii) baseline carbon residence times (τ'_E), which are usually preset in a model according to vegetation characteristics and soil types, (iii) environmental scalars (ξ), including temperature and water scalars, and (iv) environmental forcings. We applied the framework to the Australian Community Atmosphere Biosphere Land Exchange (CABLE) model to help understand differences in modeled carbon processes among biomes and as influenced by nitrogen processes. With the climate forcings of 1990, modeled evergreen broadleaf forest had the highest NPP among the nine biomes and moderate residence times, leading to a relatively high carbon storage capacity (31.5 kg cm^{-2}). Deciduous needle leaf forest had the longest residence time (163.3 years) and low NPP, leading to moderate carbon storage (18.3 kg cm^{-2}). The longest τ_E in deciduous needle leaf forest was ascribed to its longest τ'_E (43.6 years) and small ξ (0.14 on litter/soil carbon decay rates). Incorporation of nitrogen processes into the CABLE model decreased X_{ss} in all biomes via reduced NPP (e.g., −12.1% in shrub land) or decreased τ_E or both. The decreases in τ_E resulted from nitrogen-induced changes in τ'_E (e.g., −26.7% in C_3 grassland) through carbon allocation among plant pools and transfers from plant to litter and soil pools. Our framework can be used to facilitate data model comparisons and model intercomparisons via tracking a few traceable components for all terrestrial carbon cycle models. Nevertheless, more research is needed to develop tools to decompose NPP and transient dynamics of the modeled carbon cycle into traceable components for structural analysis of land models.

Keywords: benchmarking analysis, biome, carbon and nitrogen coupling, model intercomparison, traceability, vegetation type

Received 7 December 2012 and accepted 30 January 2013

Introduction

To simulate ecological responses to global change as realistically as possible, land models have incorporated more and more relevant processes in the past decades. For example, the number of key state variables in the Terrestrial Ecosystem Model (TEM) was only five in its first version (Raich *et al*., 1991), and has increased to more than 20 in its successor model – Dynamic Land Ecosystem Model (DLEM) (Tian *et al*., 2012). The Community Land Model (CLM) has recently incorporated the carbon–nitrogen cycle, transient land-cover change, and wood harvest, among many other processes, into its latest version (Oleson *et al*., 2010; Lawrence *et al*., 2011). The more processes a land model incorporates to realistically simulate real-world phenomena, the more difficult it becomes to understand or evaluate complex behaviors of the land model. As a result, uncertainty in predictions among models cannot be easily diagnosed and attributed to its sources (Chatfield, 1995; Friedlingstein *et al*., 2006; Luo *et al*., 2009). For example, simulated land carbon uptake in response to doubled CO_2 concentration in the atmosphere varied from 100 to 800 GtC among 11 coupled climate–carbon cycle models (Friedlingstein *et al*., 2006). Simulated annual net primary productivity (NPP) ranged from 39.9 Pg C yr^{-1} by the HYBRID model to 80.5 Pg C yr^{-1} by the Terrestrial Uptake and Release of Carbon (TURC) model among 17 models (Cramer *et al*., 1999). Although the ensemble averages of simulations from multimodels intercomparisons generally fit data better than individual models (Hanson *et al*., 2004; Dirmeyer *et al*., 2006; Johns *et al*., 2011), there is no effective approach to help identify sources of uncertainties among models.

Efforts have been made to understand the complexity of ecosystem models for model evaluation and

Correspondence: Jianyang Xia, Department of Botany and Microbiology, University of Oklahoma, Norman, OK 73019, USA, tel. + 1 405 325 6519, fax + 1 405 325 8578 e-mail: jxia@ou.edu

intercomparison. For example, Wang *et al.* (2011a) has developed a hierarchical framework that segregates ecosystem models into three functionally cascaded components, which are as follows: (i) how climate drivers and vegetation leaf area influence NPP, (ii) how NPP allocation and plant carbon turnover rates together determine biomass growth, and (iii) how soil carbon balance is determined by the carbon input from litter fall and carbon loss via heterotrophic respiration. By examining the three components sequentially, that framework is useful for diagnosing and assessing uncertainties of simulated carbon fluxes and storage among different models. However, the framework cannot trace the uncertainties among models to their origins in a rigorous way. For example, differences in heterotrophic respiration among models could result from the differences in sizes or turnover rates of various carbon pools. The framework by Wang *et al.* (2011a) could not differentiate them. Other intercomparison studies have made attempts to explain uncertainties among models, but mostly in descriptive rather than analytic ways.

The terrestrial carbon cycle can be decomposed into a few traceable components according to its fundamental properties. Carbon from the atmosphere enters ecosystems via photosynthesis. Once the carbon is assimilated, it is partitioned into various plant pools and transferred to litter and soil pools. Carbon is eventually released back to the atmosphere via respiration. All the carbon cycle processes after photosynthesis can be summarized by ecosystem carbon residence time, which measures an averaged duration of carbon atoms from the entrance via photosynthesis to the exit via respiration from various pools of the ecosystem (Thompson *et al.*, 1996; Luo *et al.*, 2003). As the carbon cycle continuously goes on, the steady-state carbon storage of a terrestrial ecosystem is jointly determined by the ecosystem carbon influx and residence time (Luo *et al.*, 2003). Indeed, the capacity of an ecosystem to store carbon can be given as the product of carbon influx (e.g., NPP) and residence time (τ_E) of the ecosystem (Taylor & Lloyd, 1992; Thompson *et al.*, 1996; Thompson & Randerson, 1999).

Carbon residence time (τ_E), however, has been much less studied than NPP, largely because residence time involves multiple processes mainly related to carbon transfer among pools and carbon release from each pool via decomposition and respiration. Decomposition of carbon compounds is determined by physical and chemical properties of carbon substrates and influenced by temperature and moisture. For instance, litter lignin fractions and carbon-to-nitrogen ratios are very important in influencing decomposition rates of plant detritus (Melillo *et al.*, 1982; Davidson & Janssens, 2006). Soil texture, such as clay content, and physical and biochemical protection considerably regulate decomposition of soil organic carbon (Trumbore *et al.*, 1996). Hence, litter chemical composition and soil properties together determine the maximum potential of the carbon release rate from an ecosystem via decomposition at optimal temperature and moisture conditions. The maximum potential is inversely related to baseline residence time of carbon in the ecosystem (τ'_E).

The potential decomposition rate is usually modified by external climate factors, such as temperature and precipitation (Burke *et al.*, 2003), so that the ecosystem (or actual) carbon residence time (τ_E) is always longer than its baseline value (τ'_E). The idea with the potential decomposition rate modified by environmental conditions has been incorporated into most biogeochemical models to simulate the carbon cycle in the terrestrial ecosystems. For example, the maximum decomposition rates of soil organic carbon are functions of soil texture in most terrestrial biogeochemical models, e.g., the CENTURY (Parton *et al.*, 1987) and CASA (Randerson *et al.*, 1997) model. Temperature effect on decomposition rates is expressed by a function of air temperature in both CENTURY (Parton *et al.*, 1987) and Roth-C model (Coleman & Jenkinson, 1999). In short, the ecosystem carbon residence time (τ_E) in almost all land models is determined by and thus can be decomposed to the product of baseline carbon residence time (τ'_E) and an environmental scalar, which links external climate factors such as precipitation and air temperature to carbon processes.

Here, we introduce a framework to decompose a complex land model into traceable components. Specifically, the framework traces modeled ecosystem carbon storage capacity (X_{ss}) to (i) a product of NPP and ecosystem residence time (τ_E). The latter τ_E can be further traced to (ii) baseline carbon residence times (τ_E), which are usually preset in a model according to vegetation characteristics and soil types, (iii) environmental scalars (ξ) including temperature and water scalars, and ultimately to (iv) the external climate forcings. In this study, we applied the framework to the Australian Community Atmosphere Biosphere Land Exchange (CABLE) model to analyze how carbon storage capacities of contrasting terrestrial biomes are differently determined by the four traceable components in both carbon-only and carbon–nitrogen coupled simulations. We also discussed the uncertainty of this framework, and at last illustrated potential applications of the framework to various model evaluations and improvements. Note that this is the first part of our work to develop a traceability framework for structural analysis of land models. Beyond this study, we intend to develop methods to decompose modeled carbon influx (e.g., NPP and gross primary production – GPP)

and transient dynamics of the terrestrial carbon cycle into a few traceable components so that modeled responses of the terrestrial carbon cycle to climate change and disturbances can be better understood.

Materials and methods

The general matrix model of the terrestrial carbon cycle

The framework for decomposing modeled terrestrial carbon storage capacity into a few traceable components in this study is built upon biogeochemical principles of the terrestrial carbon cycle. The terrestrial carbon cycle can be characterized by several properties (Luo & Weng, 2011), including (i) the carbon cycle in a terrestrial ecosystem is usually initiated with plant photosynthesis; (ii) the photosynthetic carbon is first partitioned into various plant pools (i.e., leaf, root, and woody biomass) and then allocated to litter and soil pools after the plant parts die; (iii) the carbon transfers are dominated by the donor pools; and (iv) decomposition of litter and soil carbon can be described by first-order decay functions. These properties of the terrestrial carbon cycle can be mathematically represented by a matrix model (Luo *et al*., 2003) as:

$$\frac{dX(t)}{dt} = BU(t) - A\xi CX(t) \tag{1}$$

where $X(t) = (X_1(t), X_2(t),..., X_9(t))^T$ is a 9 × 1 vector describing nine carbon pool sizes in leaf, root, wood, metabolic litter, structural litter, coarse wood debris (CWD), fast, slow, and passive soil organic carbon, respectively, in the CABLE model (Wang *et al*., 2011b). $B = (b_1, b_2, b_3, 0, \ldots, 0)^T$ represents the partitioning coefficients of the photosynthetically fixed carbon into different plant pools. U is the input of fixed carbon via plant photosynthesis. C is a 9 × 9 diagonal matrix with diagonal entries given by vector $c = (c_1, c_2, \ldots, c_9)^T$, components c_j (j = 1, 2, …,9) quantify the fraction of carbon left from pool X_j (j = 1, 2, …,9) after each time step. ξ is a 9 × 9 diagonal matrix with diagonal entries given by vector $\xi' = (\xi'_1, \xi'_1, \ldots, \xi'_9)^T$ (see supplementary materials), components ξ'_j (j = 1, 2, …,9) quantify the environmental scalar on carbon decay rate of pool X_j (j = 1, 2, …,9) at each time step. A denotes the carbon transfer matrix among pools as:

$$A = \begin{pmatrix} 1 & 0 & 0 & 0 & 0 & 0 & 0 & 0 & 0 \\ 0 & 1 & 0 & 0 & 0 & 0 & 0 & 0 & 0 \\ 0 & 0 & 1 & 0 & 0 & 0 & 0 & 0 & 0 \\ -a_{41} & -a_{42} & 0 & 1 & 0 & 0 & 0 & 0 & 0 \\ -a_{51} & -a_{52} & 0 & 0 & 1 & 0 & 0 & 0 & 0 \\ 0 & 0 & 1 & 0 & 0 & 1 & 0 & 0 & 0 \\ 0 & 0 & 0 & -a_{74} & -a_{75} & -a_{76} & 1 & 0 & 0 \\ 0 & 0 & 0 & 0 & -a_{85} & -a_{86} & -a_{87} & 1 & 0 \\ 0 & 0 & 0 & 0 & 0 & 0 & -a_{97} & -a_{98} & 1 \end{pmatrix}$$

where a_{ij} represents the fraction of carbon transfer from pool j to i. In general, Eqn (1) can adequately summarize carbon cycle processes in most land models (Parton *et al*., 1987; Sitch *et al*., 2003; Wang *et al*., 2010). For example, modeled carbon loss processes such as litter decomposition and soil heterotrophic respiration can be obtained from their associated components in X, A, B, C, and ξ.

All the parameters (i.e., B, ξ, A, and C) in Eqn (1) are either preset or modeled independently from each other in almost all land models. This mutually independent property of modeled carbon cycle enables us to develop an analytic framework for decomposing modeled carbon storage capacity into traceable components as described below.

The framework for decomposing modeled carbon storage capacity into traceable components

The carbon storage capacity of an ecosystem equals the sum of carbon in all the pools at steady state. The steady-state values of all carbon pools (X_{ss}) can be obtained by letting Eqn (1) equal zero (Luo *et al*. 2001, Xia *et al*., 2012) and rearranging it as:

$$\begin{aligned} X_{ss} &= (A\xi C)^{-1}BU_{ss} = (\xi C)^{-1}A^{-1}BU_{ss} = \xi^{-1}C^{-1}A^{-1}BU_{ss} \\ &= \xi^{-1}\tau_E^t U_{ss} = \tau_E U_{ss} \end{aligned} \tag{2}$$

where X_{ss} is a vector including steady states of all carbon pools, and total ecosystem carbon storage capacity can be summed from all components of X_{ss}. U_{ss} is the ecosystem carbon influx at steady state. τ'_E is the baseline carbon residence time and is determined by partitioning (B vector) and transfer (A and C matrices) coefficients in Eqn (2) as:

$$\tau_E^t = C^{-1}A^{-1}B \tag{3}$$

The ecosystem carbon residence time (τ_E) in Eqn (2) is τ'_E modified by the environmental scalar (ξ) as:

$$\tau_E = \xi^{-1}\tau_E^t \tag{4}$$

where ξ is the environmental scalar and usually consists of temperature (ξ_τ) and water (ξ_w) scalars (Burke *et al*., 2003). For litter and soil carbon pools, ξ usually is calculated from ξ_τ and water ξ_w as:

$$\xi = \xi_T\, \xi_W \tag{5}$$

Our traceability framework is based on Eqns (2)–(5) that decompose the carbon storage capacity of an ecosystem into four traceable components (Fig. 1). First, the carbon storage capacity (X_{ss}) of a terrestrial ecosystem is the product of the

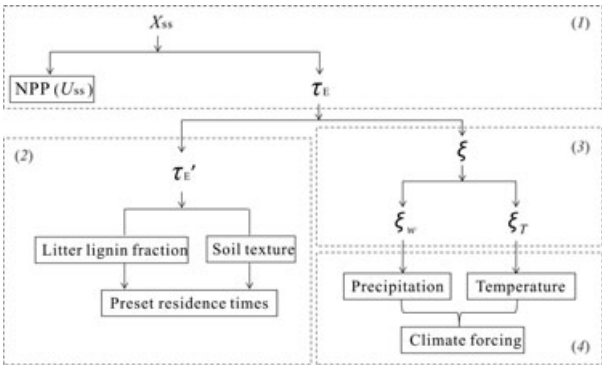

Fig. 1 Schematic diagram of the framework introduced in this study. X_{ss}, ecosystem carbon storage capacity; τ_E, ecosystem carbon residence time; τ'_E, baseline carbon residence time; ξ, environmental scalar; ξ_T, temperature scalar; ξ_W, water scalar.

ecosystem carbon residence time (τ_E) and the steady-state ecosystem carbon influx (U_{ss}) Eqn (2). According to Eqn (4), τ_E is the baseline carbon residence time (τ'_E; component 2) as modified by the environmental scalar (ξ; component 3). The baseline residence time τ'_E is determined by carbon partitioning coefficients of NPP (B vector) and transfer coefficients between carbon pools [A and C matrices; Eqn (3)]. ξ can be further divided into temperature (ξ_τ) and water (ξ_w) components [Eqn (5)]. The last component is external environmental climate forcings (surface air temperature and precipitation), which drive the carbon cycle in all terrestrial ecosystem models.

In Equation (2), parameters ξ, A, C, and B usually vary with time, given U_{ss} during a period, in most models. Thus, we need approximations, e.g., using temporal means in this study (see details in Text S3), to represent these time-varying variables in the framework.

Error in the analytical approximation

In Equation (1), environmental scalars (ξ), partitioning coefficients of NPP (B vector), and carbon decay rates (C matrix) usually vary with time in some models. In the CABLE model, time-varying variables include ξ, B, and leaf decay rate in the **C** matrix. In this study, we used the yearly means to approximate these time-varying variables (Text S4). The approximations yield errors when they are used to estimate the ecosystem carbon storage capacity. Mathematically, the error is determined by the amplitudes of periodical oscillations of ξ and B (Text S3). The larger the amplitude is, the greater the approximation errors in estimating the ecosystem carbon storage capacity. In this study, we calculated the error of our framework by using the following Eqn:

$$Error(\%) = \frac{(\hat{X}_{tot} - X_{tot})}{X_{tot}} \times 100 \qquad (6)$$

where $\hat{X}_{tot}$ is the estimated ecosystem carbon storage capacity from our framework by using the approximate ξ and **B**. X_{tot} is the total ecosystem carbon pool size obtained by model simulations at steady state.

The Community Atmosphere–Biosphere–Land Exchange (CABLE) model

Currently, biogeochemistry in most global land models are constructed on the pool–flux structure, which can be summarized into the general matrix model in this study. Here, we applied our framework to the Community Atmosphere–Biosphere–Land Exchange (CABLE) model, which is one of the land surface models that are used for simulating global biophysical processes and climate. The biogeochemical cycle of the CABLE model contains coupled carbon, nitrogen, and phosphorus cycles (Wang *et al*., 2010). In this study, we first activated the carbon cycle to introduce the framework, and then used the carbon–nitrogen coupled model to examine the impacts of carbon–nitrogen coupling on the carbon cycle.

There are nine carbon pools in the CABLE model, including three plant pools (leaf, root, and wood), three litter pools (metabolic and structural litter as well as CWD), and three soil pools (microbial biomass, slow and passive soil organic matter). Ecosystem carbon influx (i.e., NPP) is calculated as the difference between gross primary productivity (GPP) and autotrophic respiration. By spinning up the model to steady states (Xia *et al*., 2012), we obtained the steady states of NPP (U_{ss}) and carbon storage capacity (X_{ss}; component 1). In the second component of the framework, the carbon transfer coefficients (A matrix) are determined by lignin/nitrogen ratio from plant to litter pools, lignin fraction from litter to soil pools, and soil texture among soil pools (Text S1). The lignin fraction is fixed according to vegetation types and soil texture is spatially fixed in the CABLE model. In the B vector, the carbon partitioning coefficients of the photosynthetically fixed carbon into plant pools are determined by availabilities of light, water, and nitrogen (Text S1). In the C matrix, the potential decay rates of different carbon pools are first preset and vary with vegetation types, and then modified by lignin fraction and soil texture, respectively (Text. S1). The environmental scalar (ξ) regulates the leaf carbon turnover rates by cold and drought stresses on leaf senescence rate, and litter/soil carbon turnover rates via limitations of soil temperature and moisture (component 3; see details in Text S2). The vegetation types for each 1°×1° grid cell in the model were derived from the 0.5°× 0.5 IGBP classification (Loveland *et al*., 2000). The daily meteorological forcings (surface air temperature, soil temperature, and moisture; component 4) were used to integrate the full model with a time step of 1 day. As the main purpose of this study is to introduce a traceability framework but not obtain best estimates for all components in our framework, the meteorological forcings of 1990 were used to run the global version of the CABLE model to steady states. Managed ecosystems such as cropland were not included in this study as land-use changes are not simulated in this version of the CABLE model.

Procedure of analysis

To obtain the modeled carbon storage capacity, we spun up the CABLE model to steady state using the semianalytical solution (SAS) method developed by Xia *et al.* (2012). Once the model is spun up to steady state, elements of A, C, B, and ξ from all time steps in the last recycle of climate forcings (as Figure S1-S3) were stored in files to calculate averages of A, C, B, and ξ over the time span as their approximations in Eqns (1–5) (Text S4). Note that the study by Xia *et al.* (2012) described in detail organization of carbon pools and fluxes into matrices A and C, vector B (as in Text S1), and the environmental scalar (ξ; as in Text S2). The obtained averages of A, C, and B were used to calculate the baseline values of ecosystem carbon residence times (τ'_E) by Eqn (3). The τ'_E (component 2 in Fig. 1) was multiplied by averaged ξ (component 3 in Fig. 1) to calculated ecosystem carbon residence time (τ_E) by Eqn (4). The ecosystem carbon storage capacity (X_{ss}) was calculated as the product of yearly NPP (i.e., $\underline{U}_{ss}$) and τ_E [Eqn (2); component 1 in Fig. 1]. Air temperature and precipitation were directly obtained from the external climate forcings (component 4 in Fig. 1). The details of the procedures in this study can be found on this webpage: http://ecolab.ou.edu/AnaTool/modelstructure.html.

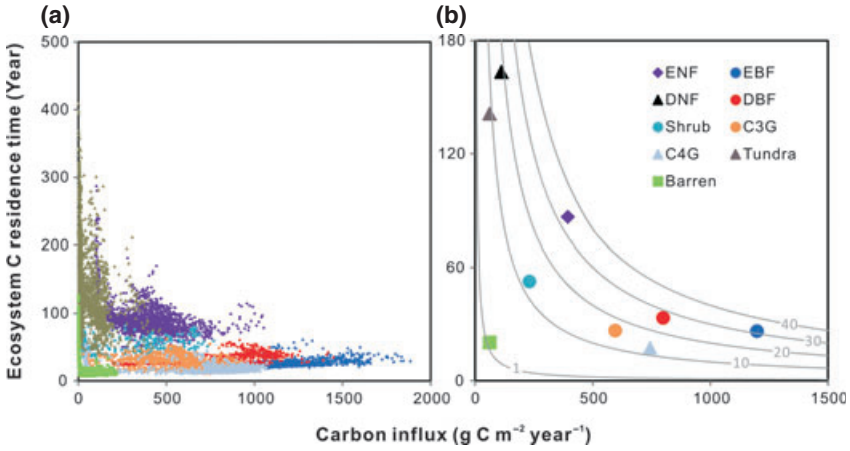

Fig. 2 Determining of the ecosystem carbon storage capacity by carbon (C) influx (i.e., NPP) and ecosystem residence time (τ_E) in various biomes. Values of all grid cells are plotted in panel (a). In panel (b), the hyperbolic curves represent constant values (shown across the curves) of ecosystem carbon storage capacity. ENF – Evergreen needle leaf forest, EBF – Evergreen broadleaf forest, DNF – Deciduous needle leaf forest, DBF – Deciduous broadleaf forest, Shrub – Shrub land, C3G – C_3 grassland, C4G – C_4 grassland, and Barren – barren/sparse vegetation.

Results

Ecosystem carbon storage capacity as determined by ecosystem residence time and NPP

According to Eqn (2), the ecosystem residence time (τ_E) and carbon influx (i.e., NPP; U_{ss}) together determine the carbon storage capacity (X_{ss}) of an ecosystem. Evergreen needle leaf forest had the largest total ecosystem carbon storage capacity (34.1 kg cm^{-2}) among the nine biomes, resulting from its mediate NPP (0.39 kg cm^{-2} yr^{-1}) and relatively long τ_E (86.4 years) (Fig. 2). Modeled evergreen broadleaf forest had the highest NPP (1.2 kg cm^{-2}) and a moderate τ_E (26.3 years), leading to a relatively high ecosystem carbon storage capacity (31.5 kg cm^{-2}). Deciduous needle leaf forest had the longest τ_E (163.3 years) and a low NPP (0.1 kg cm^{-2} yr^{-1}), resulting in a moderate ecosystem carbon storage capacity (18.3 kg cm^{-2}). Barren/sparse vegetation had the lowest ecosystem carbon storage capacity (1.3 kg cm^{-2}) among all the biomes as a result of its smallest NPP (0.1 kg cm^{-2} yr^{-1}) and shortest τ_E (20.4 years). Although tundra had a long τ_E (141.2 years), its ecosystem carbon storage capacity (8.7 kg cm^{-2}) is small because of the low NPP (0.1 kg cm^{-2} yr^{-1}).

Baseline carbon residence time

The ecosystem carbon residence time is determined by baseline carbon residence time (τ'_E) and the environmental scalar Eqn (4). Differences in τ'_E among biomes (Figs. 3a and 4) are determined by the potential decomposition rates of carbon pools (C matrix), coefficients of partitioning NPP to plant pools (B vector), and carbon transfer coefficients between pools (A matrix) [Eqn (3)]. For example, needle leaf deciduous forests had the longest τ'_E (an average of 55.7 years) of the nine biomes because they partitioned the largest fraction of NPP into woody biomass (45.0%) (Text S4). The matrices of **A** and **C** as well as the *B* vector are determined by soil texture (Fig. 3b) and vegetation lignin fraction (Fig. 3c), both of which are preset in the model (Text S1). In this study, the total fraction of clay and silt was relatively large in forests (0.55 0.67) and similar in shrub land (0.47), tundra (0.52), and barren/sparse vegetation (0.47). C_3 grassland (0.61) had a larger total fraction of clay and silt than C_4 grassland (0.50) (Fig. 3b). Plant lignin fraction was largest in evergreen needle leaf forest (0.30), but smallest in barren/sparse vegetation (0.23). It was set as 0.27 in other forests and shrub land, and 0.20 in grassland and tundra (Fig. 3c).

Climate forcings and environmental scalars

Climate forcings that drive the model are different among biomes. For example, C_4 grassland (25.8 ± 0.1 °C, 1018.6 ± 15.5 mm) had higher temperature and more precipitation than C_3 grassland (13.5 ± 0.2 °C, 874.2 ± 12.8 mm) (Table 1, Fig. 5a). Temperature and water availability limit decomposition rates of litter and soil organic carbon and, as a consequence, elongate residence times of various carbon pools. This concept is usually represented by an environmental scalar (ξ) in most biogeochemical models to convert baseline carbon residence time (τ'_E) into the actual ecosystem value (τ_E)

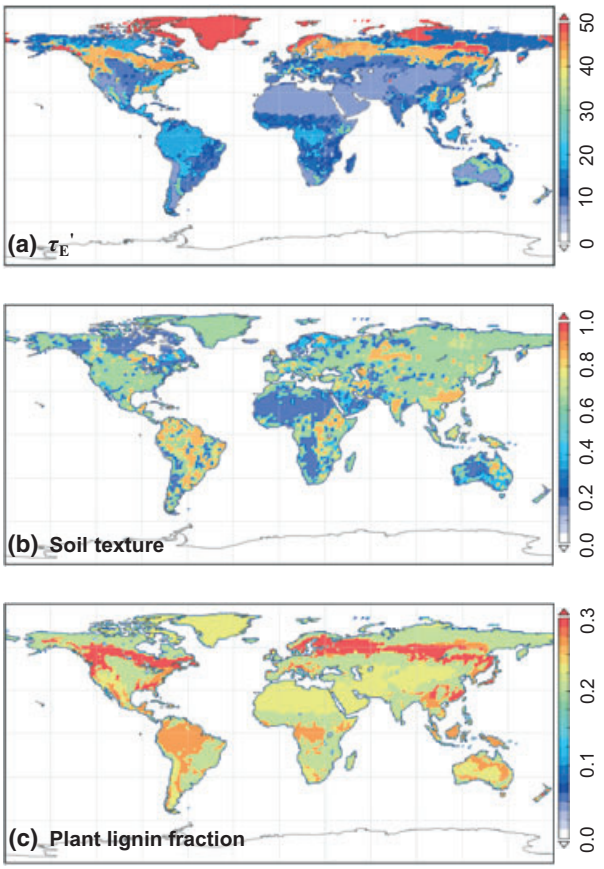

Fig. 3 Global distributions of (a) ecosystem carbon baseline residence time (τ'_E; year), (b) total fractions of clay and silt in the soil, and (c) mean plant lignin fraction. Note that we calculate the mean plant lignin fraction from leaf, root, and woody biomass without considering differences in carbon allocation pattern among grids.

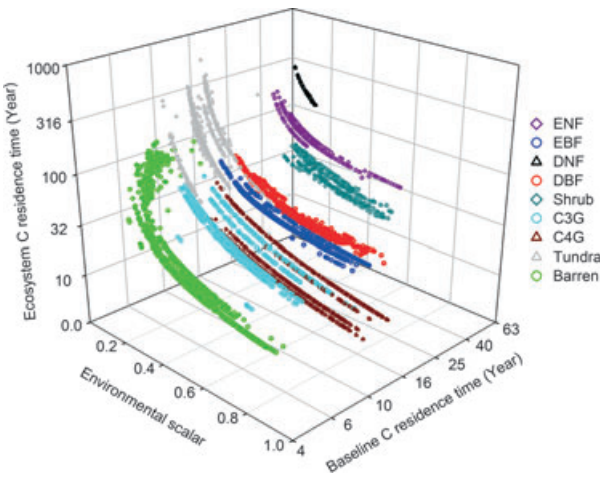

Fig. 4 Dependence of ecosystem C residence time (τ_E) on its baseline (τ'_E) and the environmental scalar (ξ) in various biomes. See abbreviations of biomes as Fig. 2.

[Eqn (3); Text S2] in each grid. In the CABLE model, for example, the smallest average value of ξ in tundra (0.13) caused the mean carbon residence time to be larger by 9.5-fold from its baseline value (Fig. 4). After the modification by ξ, the order of τ_E among biomes was different from that of τ'_E, with deciduous needle leaf forest (163.3 years) > tundra (141.2 years) > evergreen needle leaf forest (86.4 years) > shrub land (52.6 years) > deciduous broadleaf forest (33.3 years) > C_3 grassland (26.6 years) > evergreen broadleaf forest (26.3 years) > barren/sparse vegetation (20.4 years) > C_4 grassland (17.5 years).

In the CABLE model, the environmental scalar ξ influences the carbon transfer among pools in two ways (see the details in Text S2). First, when air temperature (cold stress) or water availability (drought stress) was too low, an additional fraction of leaf carbon is transferred to litter pools (from 0.87% in evergreen broadleaf forest to 16.1% in deciduous broadleaf forest; Text S4). Second, decomposition rates of litter and soil organic carbon pools all were modified by temperature (ξ_T) and water (ξ_W) scalars in the same way in the CABLE model (Text S2). In this study, the global mean values of ξ_T and ξ_W were 0.39 and 0.74, respectively. ξ_T was small in tundra (0.13), deciduous needle leaf forest (0.15), and evergreen needle leaf forests (0.23); moderate in barren/sparse vegetation (0.40), C_3 grassland (0.44), deciduous broadleaf forest (0.47); and relatively large in shrub land (0.61), evergreen broadleaf forest (0.62), and C_4 grassland (0.82) (Fig. 5 and 6). In contrast to the large variation in ξ_T among biomes, ξ_W was distributed in a narrow range from 0.65 in evergreen broadleaf forest to 0.87 in deciduous needle leaf forest (Figs. 5, 6 and S1).

Table 1 Mean annual temperature (MAT) and precipitation (MAP) in the nine biomes in 1990. The mean (SD) values were obtained from different grid cells with same biome type.

Biome	MAT	MAP
Evergreen Needle leaf Forest (ENF)	2.5 (6.2)	1005.3 (687.2)
Evergreen Broadleaf Forest (EBF)	23.9 (4.7)	2049.4 (652.2)
Deciduous Needle leaf Forest (DNF)	−7.0 (1.4)	372.4 (103.3)
Deciduous Broadleaf Forest (DBF)	16.9 (8.0)	1397.4 (531.5)
Shrub land (Shrub)	21.7 (4.2)	467.9 (203.0)
C_3 grassland (C3G)	13.5 (7.4)	874.2 (444.7)
C_4 grassland (C4G)	25.8 (2.2)	1018.6 (491.7)
Tundra	−8.0 (5.2)	598.6 (544.3)
Barren/sparse vegetation (Barren)	7.9 (17.5)	219.8 (230.7)

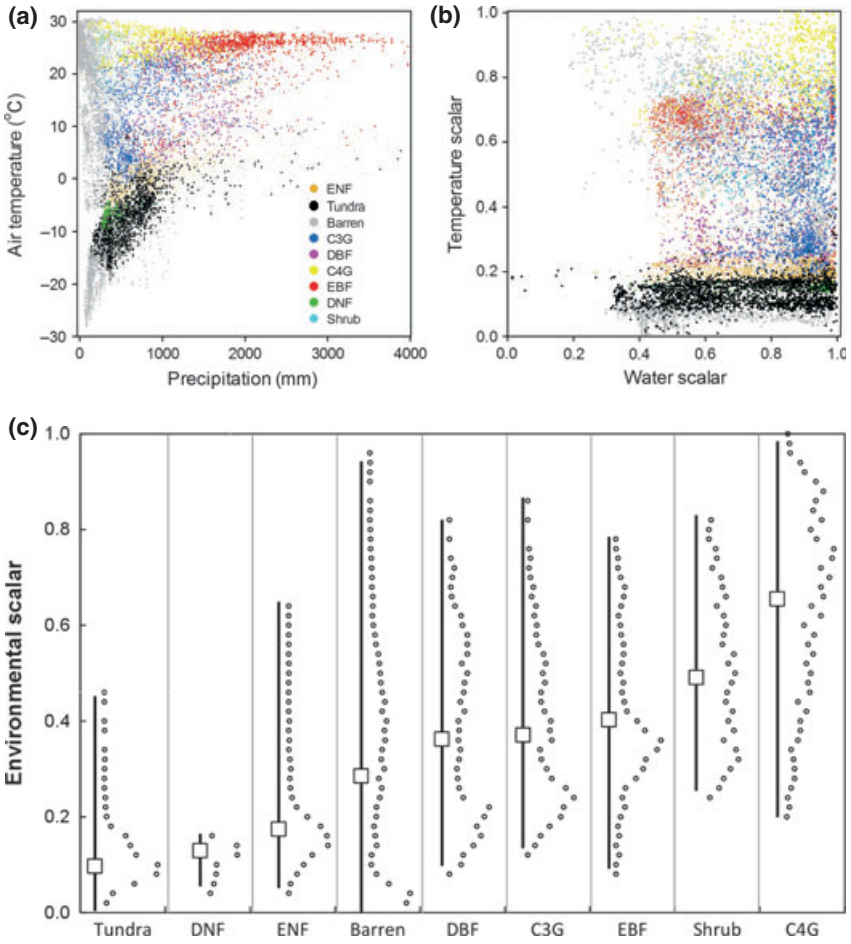

Fig. 5 Distribution of major biomes in relation to (a) annual temperature and precipitation and (b) water (ξ_W) and temperature (ξ_T) limitations on litter and soil organic carbon decomposition rates. (c) Frequency distributions of environmental scalars (ξ) on litter/soil decay rates in various biomes. The blank squares are averages of ξ, and the bars cover the range from the minimum to maximum ξ in a biome. See abbreviations of biomes as Fig. 2.

Approximation errors of the framework

Although our results showed a good agreement between analyzed and modeled ecosystem carbon storage capacity in all biomes (Fig. 7), there are some inevitable approximation errors in applying our framework from the temporal variations in environmental scalars (ξ), partitioning coefficients of NPP into plant pools (B vector), and fraction of carbon left from the leaf pool ($c1$). Among the nine biomes, the largest error occurred in deciduous needle leaf forest (7.14%) and tundra (5.11%). It was attributed to the large temporal fluctuations of partitioning coefficients of NPP into plant pools (B vector; Fig. S2) and leaf turnover rates ($c1$; Fig. S3). The error was much lower in other biomes (from -0.57% in evergreen broadleaf forest to 2.06% in deciduous broadleaf forest) because of small or no temporal variations in B, $c1$, and ξ (Figs. S1–S3). In general, the approximation errors for the ecosystem carbon storage capacity resulted mainly from two sources: (1) using $(\bar{\xi}_T \cdot \bar{\xi}_W)^{-1} \cdot \overline{\tau'_e}$ as an approximation for $\overline{\xi_T^{-1} \cdot \xi_W^{-1} \cdot \tau'_e}$, and (2) approximating $\overline{\xi_T^{-1} \cdot \xi_W^{-1}}$ by $\overline{\xi_T^{-1}} \cdot \overline{\xi_W^{-1}}$. To evaluate the first source of approximation errors, we compared values of $(\bar{\xi}_T \cdot \bar{\xi}_W)^{-1} \cdot \overline{\tau'_e}$ with values of $\overline{\xi_T^{-1} \cdot \xi_W^{-1} \cdot \tau'_e}$ for each carbon pool and biome. The approximation errors were relatively large for litter and soil pools, especially in deciduous needle leaf forest (from 5.96 to 35.69%; Fig. S4). Such a large uncertainty resulted from the great temporal variations of ξ_T^{-1}, ξ_W^{-1}, and τ'_e in this biome (Fig. S5). To evaluate the second source of approximation errors, we calculated the differences between $\bar{\xi}_T \cdot \bar{\xi}_W$ and $\overline{\xi_T \cdot \xi_W}$ for all grids. The result showed that the approximation errors were minor globally (Fig. S6). The two sources of approximation errors may vary with models so that the above uncertainty analyses should be performed before applying our framework to a model.

Although the above temporal variations are fundamental properties of terrestrial ecosystems and are the drivers for the seasonality of the modeled carbon cycle, the approximation error generated by using our framework to decompose the modeled ecosystem carbon storage capacity is relatively small.

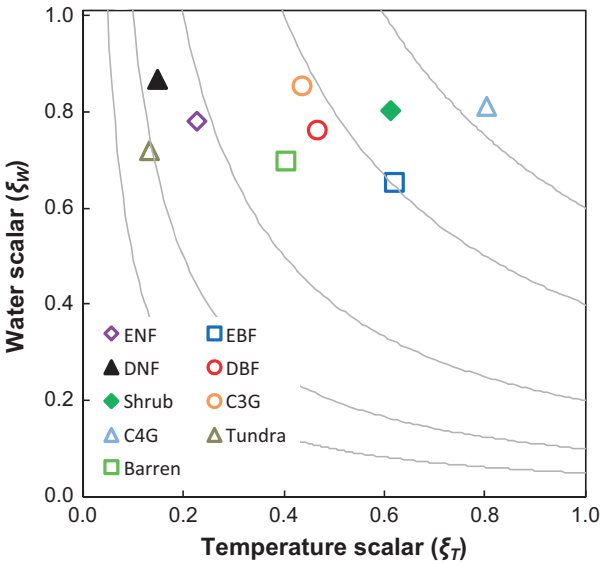

Fig. 6 Determining of the environmental scalar (ξ) by temperature (ξ_T) and water (ξ_W) scalars in different biomes. The hyperbolic curves represent constant values (shown across the curves) of ξ. See abbreviations of biomes as Fig. 2.

Nitrogen constraints of ecosystem carbon storage capacity

In the CABLE model, NPP and baseline carbon residence time (τ_E) and therefore carbon storage capacity all decreased in all biomes when the nitrogen cycle was coupled with the carbon cycle (Fig. 8b). As the environmental scalars on litter and soil carbon turnover rates are not related with nitrogen processes (Text S1), the incorporation of nitrogen processes affects τ_E only via its influences on τ'_E. The nitrogen-induced reduction in the ecosystem carbon storage capacity mainly resulted from decreased NPP in forests and shrub land and shortened τ'_E in other biomes (Fig. 8). For example, the large nitrogen-induced reduction in the ecosystem carbon storage capacity of C_3 (−34.5%) and C_4 (−23.5%) grassland resulted from the relatively large changes in τ'_E (−26.7% and −17.5%, respectively) with relatively small decreases in NPP (−3.0% and −5.2%, respectively). The incorporation of nitrogen processes had small impacts on forest carbon storage capacity (from −1.5% to −9.6%) because of its small impacts on the forest τ'_E (from −0.1% to −2.3%) and NPP (from −1.5% to −5.5%) (Fig. 8b). According to Eqn (3),

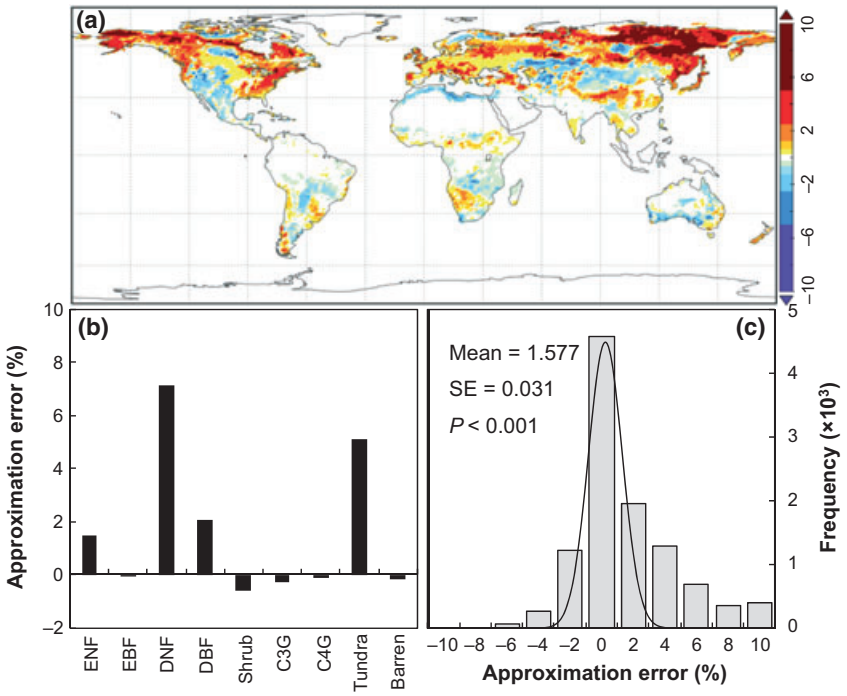

Fig. 7 (a) Global spatial distributions and (b) biome-level averages of the approximation error of analyzed against modeled total ecosystem carbon storage capacity. The solid line in panel b is 1 : 1 line. Panel c shows the frequency distribution of the approximation errors, and the solid curve is a Gaussian distribution fitted to the frequency data. See abbreviations of biomes as Fig. 2.

nitrogen regulates τ'_E via affecting A, B, and C. As the incorporation of the nitrogen cycle only slightly influenced the B vector in nonforest biomes (Text S4 and S5), its impacts on τ'_E mainly stem from its influences on the **A** and **C** matrices in this study. The incorporation of the nitrogen cycle leads to more leaf and root carbon transfers to the short-lived litter pool (metabolic litter; Text S4 and S5), and thus to a negative nitrogen effect on τ'_E in all biomes. The potential decomposition rates of soil organic carbon in the **C** matrix were increased by the nitrogen incorporation more in nonwoody than woody biomes (Text S4 and S5), leading to a larger nitrogen impact on τ'_E in nonwoody than woody biomes (Fig. 8b).

Discussions

Traceability of differences in ecosystem carbon storage capacity among biomes

Although many previous modeling studies have reported great geographic variations in the simulated ecosystem carbon storage across the globe (Cao & Woodward, 1998; Ogle *et al.*, 2010), there is no analytic approach to mechanistically explain such spatial heterogeneities. The framework introduced in this study (Fig. 1) can trace the modeled ecosystem carbon storage capacity into four components and thus help our understanding of its differences among biomes in a mechanistic way. In the CABLE model, for example, C_3 grassland had a larger carbon storage capacity than C_4 grassland, resulting from the longer ecosystem carbon residence time (τ_E) in C_3 than C_4 grassland, even though NPP was higher in C_4 than C_3 grassland (Fig. 2). C_3 grassland had a longer τ_E than C_4 grassland because of its smaller environmental scalar (ξ; Fig. 4-6) even if the baseline carbon residence time (τ'_E) was shorter in C_3 than C_4 grassland (Fig. 3 and 4). The difference in the environmental scalar (ξ) between C_3 and C_4 grassland was determined by temperature (ξ_T) but not water (ξ_W) (Figs. 5 and 6). The smaller temperature scalar (ξ_T) in C_3 than C_4 grassland (Figs. 5b and 6) is due to the fact that C_3 grassland is located in colder areas than C_4 grassland (Table 1, Fig. S4a). In this way, we traced the different carbon storage capacity between C_3 and C_4 grassland to temperature scalars and environmental forcings. Such an analysis can be easily applied to other biomes. Thus, the framework offers a mechanistic approach to explain the geographic variations in modeled carbon storage capacity.

The framework that can mathematically decompose the modeled carbon storage capacity into a few traceable components (Equations (2)–(5) and Text S3) is based on the fact that those components of the carbon cycle are simulated in the CABLE model as well as many other models in a mutually independent manner. For example, carbon influx (e.g., NPP) is simulated independently from carbon residence time, and environmental scalars (either the temperature or water scalar) are modeled independently from carbon transfer and partitioning coefficients or environmental forcings [Eqns (1)–(5) and Text S1–S5]. Thus, the framework of traceability can mechanistically attribute differences in modeled carbon cycle to variations in model structural components, which, to the best of our knowledge, has not been developed in the literature. The framework developed by Wang *et al.* (2011a) attempted to explain differences in the modeled plant biomass by its components but could not explain them in mechanistic ways as our framework does. Nevertheless, our framework can generate small errors due to asynchrony of seasonal variations in those traceable components [Eqn (S7) and Figs S2–S4].

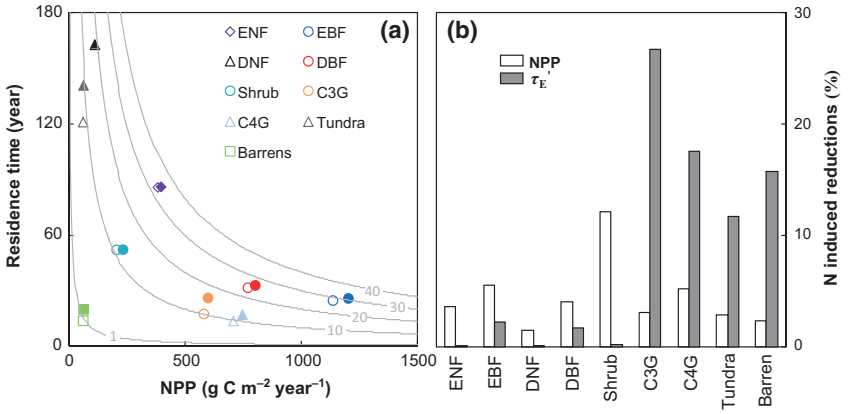

Fig. 8 Nitrogen (N)-induced changes in (a) the ecosystem carbon storage capacity and its determinants and (b) NPP and the baseline carbon residence time (τ'_E) in comparison with carbon-only simulations. In (a) panel, the filled and open symbols represent results from carbon-only and carbon–nitrogen coupled simulations, respectively. See abbreviations of biomes and notes as Fig. 2.

Effects of incorporating the nitrogen cycle into land models

Biogeochemical models have incorporated many relevant processes, such as the nitrogen cycle and dynamic vegetation, in the past decades in an attempt to simulate carbon–climate feedback as realistically as possible. Adding a new module to a land model usually triggers various impacts on existing carbon cycle processes. Such impacts have been described, but, to our knowledge, never rigorously evaluated. This study uses this traceability framework to assess the impacts of these added nitrogen processes on carbon storage capacity (Fig. 8). Incorporating the nitrogen cycle into the CABLE model reduces ecosystem carbon storage capacity in all biomes in comparison with that in the carbon-only model (Fig. 8a). In the nonforest biomes, for example, the addition of nitrogen processes resulted in the reduction in ecosystem carbon storage capacity mainly by decreasing NPP in shrub land and via shortened τ'_E in other nonwoody biomes (Fig. 8b). The larger nitrogen-induced reductions in τ'_E in those nonwoody biomes can be ascribed to more carbon transfers from plant pools to short-lived litter pools (metabolic litter pool; Text S4 and S5), and larger preset decomposition rates of soil organic carbon (**C** matrix) in the coupled nitrogen–carbon model than the carbon-only model (Text S4 and S5). In this way, our traceability framework can help examine how the incorporation of the nitrogen cycle altered the carbon cycle of different biomes and evaluate their relative importance in determining the carbon storage capacity.

The nitrogen cycle has been incorporated into several global land models, such as the Princeton-Geophysical Fluid Dynamic Laboratory (GFDL) LM3V (Gerber *et al*., 2010), CLM-CN (Oleson *et al*., 2010), and O-CN models (Zaehle *et al*., 2010), and the CABLE model (Wang *et al*., 2010). Each model represents carbon–nitrogen coupling in different ways. For example, the nitrogen demand of plant growth is differently represented in these models although all the models simulate nitrogen limitation of plant growth when nitrogen availability cannot meet plant nitrogen demand. The nitrogen demand equals the nitrogen requirement to sustain the current growth rate in the O-CN model (Zaehle *et al*., 2010); the maximal nitrogen requirement (as a product of maximal nitrogen:carbon ratio and NPP allocated to each plant pool) minus the plant resorbed nitrogen in the CABLE model (Wang *et al*., 2010) and a fraction of the total annual nitrogen demand for the previous year in the CLM-CN model (Oleson *et al*., 2010). The different representations of nitrogen demand will induce different impacts on NPP in these models. Moreover, the incorporation of the nitrogen cycle can differently affect the baseline carbon residence time (τ'_E) in these models. For example, the carbon transfer coefficients (**A** matrix) are constant in the CLM-CN model (Oleson *et al*., 2010), but vary with the nitrogen availability in other models. When the nitrogen cycle is incorporated, more plant carbon transfers to a short-lived litter pool in the O-CN (Zaehle *et al*., 2010) and CABLE (Wang *et al*., 2010) models whereas less litter carbon transfers to the recalcitrant soil carbon pool in the LM3V model (Gerber *et al*., 2010). Our traceability framework can help evaluate the relative importance of those different carbon–nitrogen coupling methods in influencing carbon storage capacities among models.

Potential applications of the framework for model evaluation and improvement

Most biogeochemical models, e.g., CENTURY (Parton *et al*., 1987), RothC (Coleman & Jenkinson, 1999), LPJ (Sitch *et al*., 2003), and Biome-BGC (Potter *et al*., 1993), share a similar structure for the carbon cycle with the CABLE model. Thus, our framework not only can be used to compare carbon storage capacity among biomes as is done in this study but also facilitate model intercomparison, benchmark analysis, and data assimilation.

Model intercomparison. Most of the model intercomparison studies have found that the ensemble means of multiple model simulations fit observations best, although variations among models are substantial, leading to great uncertainties in model predictions (e.g., Hanson *et al*., 2004). For example, Friedlingstein *et al*. (2006) have compared climate–carbon cycle feedbacks among 11 coupled climate–carbon cycle models, and found a large range of climate impacts on the land carbon storage. However, there is no effective approach to trace such uncertainties to their sources. Our framework has the potential to explain model variations in a very simple way with a few traceable components. If all the information of NPP, **A**, **C**, **B** and ξ [Eqn (1)] at steady states is collected from different models in the form of Text S1–S5, we can easily apply this traceability framework to trace the model uncertainties to their sources.

Benchmarking complex land models. Multiple observations are used as benchmarks to evaluate performances of complex land models (Luo *et al*., 2012). Many statistical approaches, such as normalized mean absolute error, the reduced χ^2 statistic, and Taylor skill (Schwalm *et al*., 2010), have been developed to measure the mismatches of modeled carbon processes with multiple observations. Besides the statistical approaches, the

Carbon-LAnd Model Intercomparison Project (C-LAMP) (Randerson *et al.*, 2009) has developed a scoring system for evaluating climate–carbon models by using nine different metrics. However, most of those approaches treated all metrics as equally important and ignore the relative contributions of different metrics to model performance. Our framework can evaluate the relative importance of various processes (or model components) in influencing carbon storage capacity. The relative importance of various model components as in Eqns (2)–(5) and Fig. 1 of this study can be used as metrics for the carbon cycle to design weighting factors for each of the processes (Luo *et al.*, 2012). Thus, the traceability framework described in this study could make the benchmarking analysis more objective.

Data assimilation. Recently data assimilation has been used to improve models and reduce uncertainties of their predictions by systematically combining observations with the models (Luo & Weng, 2011; Weng & Luo, 2011; Zobitz *et al.*, 2011). It can quantitatively project the misfit between model and observations instead of judging model performance by several given criteria. However, a data assimilation system cannot include all parameters and state variables because of some practical reasons, such as data availability and computational requirements. As a consequence, presently data assimilation techniques are usually implemented into a site-level model for improving a few target variables, e.g., ecosystem CO_2 exchange (Xu *et al.*, 2006; Zhou *et al.*, 2010; Zobitz *et al.*, 2011), but are difficult to implement to improve the comprehensive carbon cycle of a global-scale land model. Our framework can help isolate major sources of model uncertainties in the four traceable components (Fig. 1), and thus identify those components with the largest contribution to the disagreement between the model and observations. Then we can focus our data assimilation on reducing uncertainties of these components by collecting relevant data sets and understanding uncertainties in associated parameters and state variables. In this way, our framework can compartmentalize the applications of data assimilation techniques to those more uncertain model components.

Future research needs on traceability of the terrestrial carbon cycle

Future research is needed to further develop this traceability framework for the structural analysis of land models. First, the framework presented in this study does not decompose NPP into its traceable components (Fig. 1) partly because many data sets are available from observations for benchmarking modeled NPP (Luo *et al.*, 2012). However, NPP has been modeled in various ways by different models, and a large uncertainty of modeled NPP simulation still exists (Schaefer *et al.*, 2012). Thus, decomposing modeled NPP into a few traceable components will be helpful for evaluating and improving land models in the future. Second, as the framework presented in this study is based on the assumption of steady state ($\frac{dX(t)}{dt} = 0$; Equation 1), it cannot directly assess the uncertainty of model simulations for transient dynamics of the terrestrial carbon cycle in response to climate change (Rogelj *et al.*, 2012) and disturbances (Prentice *et al.*, 2011). It is crucial to further develop the traceability framework to decompose the transient carbon cycle into a few traceable components.

As the framework separates the relative contributions of NPP and carbon residence time to ecosystem carbon storage, it can improve not only model evaluations but also model usability and interpretation. For example, we can assess relative costs and trade-off strategies of carbon sequestration pathways to increase carbon storage through either longer carbon residence times or higher NPP, and find the best pathways to enhance carbon sequestration in different regions. In addition, the framework can help us figure out how various processes influence the ecosystem carbon storage capacity through changes in NPP and carbon residence times. For example, changes in nitrogen availability (e.g., nitrogen deposition and fertilization) mainly impact the ecosystem carbon storage capacity through NPP in woody biomes (forests and shrub land), but through carbon residence times in other biomes (Fig. 8). Thus, although the framework cannot evaluate the transient terrestrial carbon cycle response to external climate change and disturbances, it can help us better understand the response mechanisms of the terrestrial carbon storage capacity to future environmental changes.

To fully understand their performance in a transparent way, it is imperative to decompose complex land models into traceable components. In this study, we decomposed a global land model of coupled carbon–nitrogen cycles into four traceable components. Specifically, we can trace the modeled ecosystem carbon storage capacity (X_{ss}) to (i) a product of net primary productivity (NPP) and the ecosystem carbon residence time (τ_E), the latter τ_E is further traced to (ii) the baseline carbon residence times (τ'_E) which are preset in a model, (iii) environmental scalars (ξ), and (iv) environmental forcings. The traceability framework has been successfully applied to the CABLE model to help us understand the modeled carbon storage capacity as varying among biomes and as affected by nitrogen processes. For example, C_3 grassland had a larger carbon storage capacity than C_4 grassland, resulting from the longer carbon residence time (τ_E) in C_3 than C_4 grassland because the C_3 grassland is located in colder areas

and thus has a smaller temperature scalar than C_4 grassland. Incorporating the nitrogen cycle into the CABLE model reduces ecosystem carbon storage capacity in woody biomes mainly by decreasing NPP and via shortening τ'_E in nonwoody biomes. The traceable components were mathematically defined from the first-order, ordinary differential matrix equation [Eqn (1)] developed by Luo *et al.* (2003). The matrix equation becomes decomposable into traceable components because those components are simulated in a mutually independent manner [Eqns (2)–(5)]. Small errors in the traceability framework (Fig. 7) arise from asynchrony of seasonal variations in those components [Eqns (S1)–(S11) and Figs. S2–S4].

The matrix equation [Eqn (1)] adequately describes almost all of the observed carbon processes, such as litter decomposition and soil C dynamics in the real world. These carbon processes have been represented in almost all ecosystem biogeochemical models, and integrated into Earth system models (Luo & Weng, 2011). As a consequence, our traceability framework should be universally applicable to almost all land models to mechanistically explain structural differences in the modeled carbon cycle. Thus, this framework not only can help understand variations in the modeled ecosystem carbon storage capacity among biomes and as affected by nitrogen processes, but also facilitate model intercomparisons and model–data comparisons to improve model performances through benchmark analyses and data assimilation.

Acknowledgments

The authors thank two anonymous reviewers and Drs. S. Niu and D. Li for their valuable suggestions, and N. Mikle for polishing language for this manuscript. This research was financially supported by US National Science Foundation (NSF) grant DBI 0850290, EPS 0919466, DEB 0743778, DEB 0840964, EF 1137293. Part of the model runs were performed at the Supercomputing Center for Education & Research (OSCER), University of Oklahoma.

References

Burke IC, Kaye JP, Bird SP, Hall SA, McCulley RL, Sommerville GL (2003) *Evaluating and testing models of terrestrial biogeochemistry: the role of temperature in controlling decomposition*, pp. 225–253. Models in ecosystem science Princeton University Press, Princeton, New Jersey, USA.

Cao M, Woodward FI (1998) Net primary and ecosystem production and carbon stocks of terrestrial ecosystems and their responses to climate change. *Global Change Biology*, **4**, 185–198.

Chatfield C (1995) Model uncertainty, data mining and statistical inference. *Journal of the Royal Statistical Society, Series A (Statistics in Society)*, **158**, 419–466.

Coleman K, Jenkinson D (1999) *ROTHC-26.3, A model for the turnover of carbon in soil: Model description and User's guide*. Herts, Rothamsted Research, Harpenden, Hertfordshire, UK.

Cramer W, Kicklighter DW, Bondeau A *et al.* (1999) Comparing global models of terrestrial net primary productivity (NPP): overview and key results. *Global Change Biology*, **5**, 1–15.

Davidson EA, Janssens IA (2006) Temperature sensitivity of soil carbon decomposition and feedbacks to climate change. *Nature*, **440**, 165–173.

Dirmeyer PA, Koster RD, Guo ZC (2006) Do global models properly represent the feedback between land and atmosphere? *Journal of Hydrometeorology*, **7**, 1177–1198.

Friedlingstein P, Cox P, Betts R *et al.* (2006) Climate-carbon cycle feedback analysis: Results from the C4MIP model intercomparison. *Journal of Climate*, **19**, 3337–3353.

Gerber S, Hedin LO, Oppenheimer M, Pacala SW, Shevliakova E (2010) Nitrogen cycling and feedbacks in a global dynamic land model. *Global Biogeochemical Cycles*, **24**, GB1001, doi:10.1029/2008GB003336

Hanson PJ, Amthor JS, Wullschleger SD *et al.* (2004) Oak forest carbon and water simulations: model intercomparisons and evaluations against independent data. *Ecological Monographs*, **74**, 443–489.

Johns TC, Royer JF, Hoschel I *et al.* (2011) Climate change under aggressive mitigation: the ENSEMBLES multi-model experiment. *Climate Dynamics*, **37**, 1975–2003.

Lawrence DM, Oleson KW, Flanner MG *et al.* (2011) Parameterization Improvements and Functional and Structural Advances in Version 4 of the Community Land Model. *Journal of Advances in Modeling Earth Systems*, **3**, M03001.

Loveland T, Reed B, Brown J, Ohlen D, Zhu Z, Yang L, Merchant J (2000) Development of a global land cover characteristics database and IGBP DISCover from 1 km AVHRR data. *International Journal of Remote Sensing*, **21**, 1303–1330.

Luo Y, Weng E (2011) Dynamic disequilibrium of the terrestrial carbon cycle under global change. *Trends in Ecology & Evolution*, **26**, 96–104.

Luo Y, Wu L, Andrews JA, White L, Matamala R, Schafer KVR, Schlesinger WH (2001) Elevated CO_2 differentiates ecosystem carbon processes: Deconvolution analysis of Duke Forest FACE data. *Ecological Monographs*, **71**, 357–376.

Luo YQ, White LW, Canadell JG *et al.* (2003) Sustainability of terrestrial carbon sequestration: A case study in Duke Forest with inversion approach. *Global Biogeochemical Cycles*, **17**, 1021 doi:1010.1029/2002GB001923.

Luo Y, Weng E, Wu X, Gao C, Zhou X, Zhang L (2009) Parameter identifiability, constraint, and equifinality in data assimilation with ecosystem models. *Ecological Applications*, **19**, 571–574.

Luo Y, Randerson J, Abramowitz G *et al.* (2012) A framework of benchmarking land models. *Biogeosciences*, **9**, 3857–3874.

Melillo JM, Aber JD, Muratore JF (1982) Nitrogen and Lignin Control of Hardwood Leaf Litter Decomposition Dynamics. *Ecology*, **63**, 621–626.

Ogle SM, Breidt F, Easter M, Williams S, Killian K, Paustian K (2010) Scale and uncertainty in modeled soil organic carbon stock changes for US croplands using a process-based model. *Global Change Biology*, **16**, 810–822.

Oleson KW, Lawrence DM, Gordon B *et al.* (2010) Technical description of version 4.0 of the Community Land Model (CLM).

Parton WJ, Schimel DS, Cole CV, Ojima DS (1987) Analysis of Factors Controlling Soil Organic-Matter Levels in Great-Plains Grasslands. *Soil Science Society of America Journal*, **51**, 1173–1179.

Potter CS, Randerson JT, Field CB, Matson PA, Vitousek PM, Mooney HA, Klooster SA (1993) Terrestrial ecosystem production: a process model based on global satellite and surface data. *Global Biogeochemical Cycles*, **7**, 811–841.

Prentice IC, Kelley DI, Foster PN, Friedlingstein P, Harrison SP, Bartlein PJ(2011) Modeling fire and the terrestrial carbon balance. *Global Biogeochemical Cycles*, **25**, GB3005.

Raich JW, Rastetter EB, Melillo JM *et al.* (1991) Potential Net Primary Productivity in South-America - Application of a Global-Model. *Ecological Applications*, **1**, 399–429.

Randerson JT, Thompson MV, Conway TJ, Fung IY, Field CB (1997) The contribution of terrestrial sources and sinks to trends in the seasonal cycle of atmospheric carbon dioxide. *Global Biogeochemical Cycles*, **11**, 535–560.

Randerson JT, Hoffman FM, Thornton PE *et al.* (2009) Systematic assessment of terrestrial biogeochemistry in coupled climate–carbon models. *Global Change Biology*, **15**, 2462–2484.

Rogelj J, Meinshausen M, Knutti R (2012) Global warming under old and new scenarios using IPCC climate sensitivity range estimates. *Nature Climate Change*, **2**, 248–253.

Schaefer K, Schwalm CR, Williams C *et al.* (2012) A model-data comparison of gross primary productivity: Results from the North American Carbon Program site synthesis. *Journal of Geophysical Research*, **117**, G03010.

Schwalm CR, Williams CA, Schaefer K *et al.* (2010) A model-data intercomparison of CO_2 exchange across North America: Results from the North American Carbon Program site synthesis. *Journal of Geophysical Research*, **115**, G00H05.

Sitch S, Smith B, Prentice IC *et al.* (2003) Evaluation of ecosystem dynamics, plant geography and terrestrial carbon cycling in the LPJ dynamic global vegetation model. *Global Change Biology*, **9**, 161–185.

Taylor JA, Lloyd J (1992) Sources and Sinks of Atmospheric CO_2. *Australian Journal of Botany*, **40**, 407–418.

Thompson MV, Randerson JT (1999) Impulse response functions of terrestrial carbon cycle models: method and application. *Global Change Biology*, **5**, 371–394.

Thompson MV, Randerson JT, Malmstr6 m CM (1996) Change in net primary production and heterotrophic respiration: How much is necessary to sustain. *Global Biogeochemical Cycles*, **10**, 711–726.

Tian HQ, Chen GS, Zhang C *et al.* (2012) Century-Scale Responses of Ecosystem Carbon Storage and Flux to Multiple Environmental Changes in the Southern United States. *Ecosystems*, **15**, 674–694.

Trumbore SE, Chadwick OA, Amundson R (1996) Rapid exchange between soil carbon and atmospheric carbon dioxide driven by temperature change. *Science*, **272**, 393–396.

Wang YP, Law RM, Pak B (2010) A global model of carbon, nitrogen and phosphorus cycles for the terrestrial biosphere. *Biogeosciences*, **7**, 2261–2282.

Wang WL, Dungan J, Hashimoto H, Michaelis AR, Milesi C, Ichii K, Nemani RR (2011a) Diagnosing and assessing uncertainties of terrestrial ecosystem models in a multimodel ensemble experiment: 2. *Carbon balance. Global Change Biology*, **17**, 1367–1378.

Wang YP, Kowalczyk E, Leuning R *et al.* (2011b) Diagnosing errors in a land surface model (CABLE) in the time and frequency domains. *Journal of Geophysical Research-Biogeosciences*, **116**, G01034 doi:01010.01029/02010JG001385.

Weng E, Luo Y (2011) Relative information contriution of model vs. data to short- and long-term forecasts of forests carbon dynamics. *Ecological Applications*, **21**, 1490–1505.

Xia J, Luo Y, Wang Y, Weng E, Hararuk O (2012) A semi-analytical solution to accelerate spin-up of a coupled carbon and nitrogen land model to steady state. *Geoscientific Model Development*, **5**, 1259–1271.

Xu T, White L, Hui D, Luo Y (2006) Probabilistic inversion of a terrestrial ecosystem model: Analysis of uncertainty in parameter estimation and model prediction. *Global Biogeochemical Cycles*, **20**, GB2007.

Zaehle S, Friend AD, Friedlingstein P, Dentener F, Peylin P, Schulz M(2010) Carbon and nitrogen cycle dynamics in the O-CN land surface model: 2. Role of the nitrogen cycle in the historical terrestrial carbon balance. *Global Biogeochemical Cycles*, **24**, GB1006, doi:10.1029/2009GB003522.

Zhou X, Luo Y, Gao C, Verburg PSJ, Arnone JA III, Darrouzet-Nardi A, Schimel DS (2010) Concurrent and lagged impacts of an anomalously warm year on autotrophic and heterotrophic components of soil respiration: a deconvolution analysis. *New Phytologist*, **187**, 184–198.

Zobitz J, Desai A, Moore DJP, Chadwick M (2011) A primer for data assimilation with ecological models using Markov Chain Monte Carlo (MCMC). *Oecologia*, **167** (3), 599–611.

Supporting Information

Additional Supporting Information may be found in the online version of this article:

Text S1. Determinants of baseline residence times (component 3 of the traceability framework) in the CABLE model.
Text S2. Environmental scalars (ξ) that modify the residence times from baseline to actual values in the CABLE model (component 2 of the traceability framework).
Text S3. Mathematical derivation for the uncertainty of the framework.
Text S4. Approximations for A, B, C, and ξ of different biomes in the framework.
Text S5. Approximations for A, B, and C of different biomes when nitrogen cycle was coupled with carbon cycle.
Figure S1. Temporal dynamics of temperature (a; ξ_T) and water (b; ξ_W) scalars on litter/soil decay rates in various biomes. See abbreviations of biomes as Table 1.
Figure S2. Temporal dynamics of partitioning coefficients from NPP to leaf (b_1), root (b_2), and wood (b_3) in various biomes.
Figure S3. Temporal dynamics of leaf potential turnover rates (c_{leaf}; day 1) in the C matrix in Eqns (1)–(6).
Figure S4. Approximation errors of using $\bar{\xi}_T^{-1} \cdot \bar{\xi}_W^{-1} \cdot \bar{\tau}_e'$ to represent $\overline{\xi_T^{-1} \cdot \xi_W^{-1} \cdot \tau_e'}$ for carbon pools in each biome. See abbreviations of biomes as Table 1. Mlitter, metabolic litter; Slitter, structural litter; CWD, coarse wood debris; FSOM, fast SOM; SSOM, slow SOM; PSOM, passive SOM.
Figure S5. Temporal dynamics of baseline carbon residence time (τ'_E; year) for each litter and soil pool in each biome.
Figure S6. Approximation errors of using $\bar{\xi}_T \cdot \bar{\xi}_W$ to represent $\overline{\xi_T \cdot \xi_W}$ in all grids from the global simulation.